Supplementary Information (SI) for Soft Matter.

Supporting information
for
CO_2-induced Drastic Decharging of Dielectric Surfaces in Aqueous Suspensions

Peter Vogel[1]*, David Beyer[2], Christian Holm[2], and Thomas Palberg[1]

[1] Institute of Physics, Johannes Gutenberg University, 55128 Mainz, Germany

[2] Institut für Computerphysik (ICP), Universität Stuttgart, 70569 Stuttgart, Germany

* corresponding author

1. Additional Data from evaluation.

In Fig. S1 we show the results for the charge ratio as obtained from the fits of Eqn (5) to the NaOH titration data in the limit of small amounts of added NaOH. The error bars represent the standard error of the fits at a confidence level of 0.95 and are smaller than the symbol size. The charge ratio Z_σ/Z as averaged over these four experiments is 0.23±0.01, where the error now represents the standard deviation. Taking the number of acidic surface groups, $N = 134 \times 10^3$, we obtain a degree of dissociation of $\alpha_{eff} = Z/N = 0.018$.

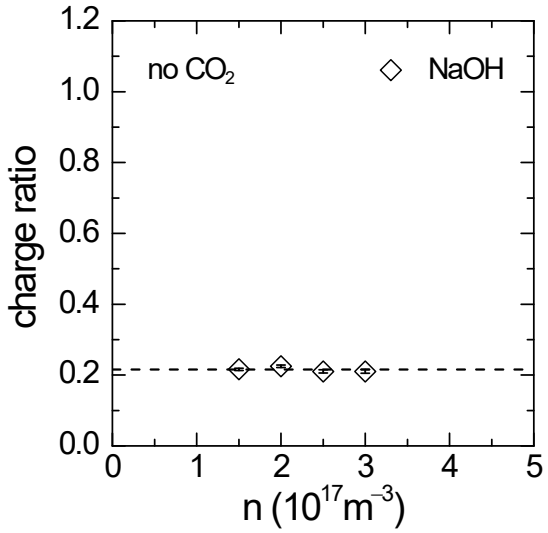

Figure S1 charge ratio Z_σ/Z obtained from conductivity titration. Error bars represent the standard errors of Fits of Eqn (5) to the data at low values of added base. The dashed line denotes the average value of $Z_\sigma/Z = 0.23\pm0.01$.

Figures S2 to S4 give a step by step illustration of our data treatment. In Fig. S2a to d, we show the data of Fig. 4 replotted on adjusted scales in dependence on the number of micro-ions added per particle, *M*. The resulting slopes show a significant dependence on the number density *n.* Moreover, the difference between initial and final slopes gets enhanced in this drawing.

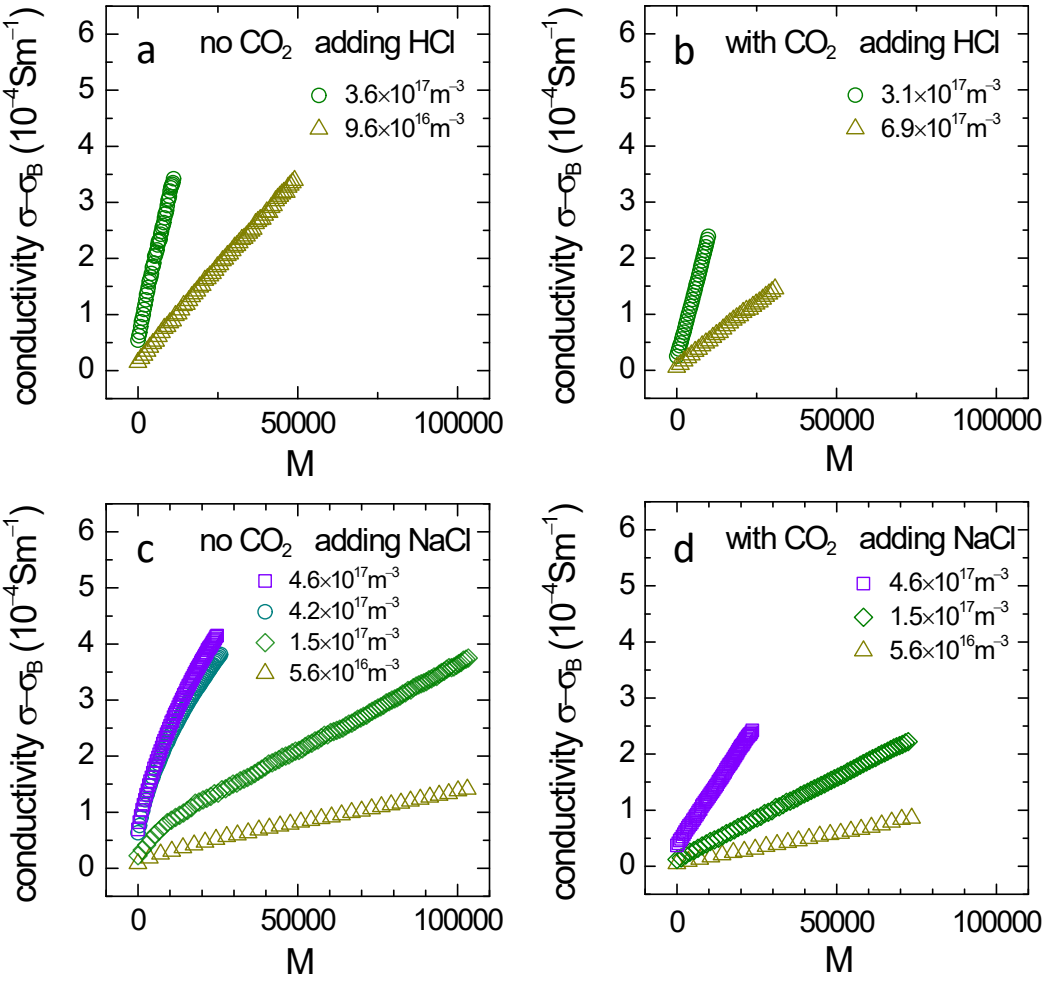

Figure S2 Background-corrected conductivity in dependence on added electrolyte per particle. Starting conditions and type of added electrolyte are indicated in each key.

In Fig. S3 we show the data for all four experiments after normalizing the conductivity by the particle number density. The semi-logarithmic plot of Fig. S3 shows the collapse onto single master curves over several orders of magnitude. In the limit $M \rightarrow 0$, data points approach constant values related to the respective particle effective charge, Z_σ, in absence or presence of CO_2.

The background and particle contribution corrected conductivity normalized by the particle density is shown in Fig. S4 in dependence on *M*. This isolates the conductivity contribution of the electrolyte per particle. Fig. S4 again highlights the differences in curve shape and clearly shows the presence of ion exchange only in the case of adding NaCl to a deionized and decarbonized system (Fig. S4c). In all

other cases the conductivity increases linearly with *M*. Note that in Fig. S4b, one observes a marginally significant deviation from the expected slope, becoming visible for the largest amounts of added HCl.

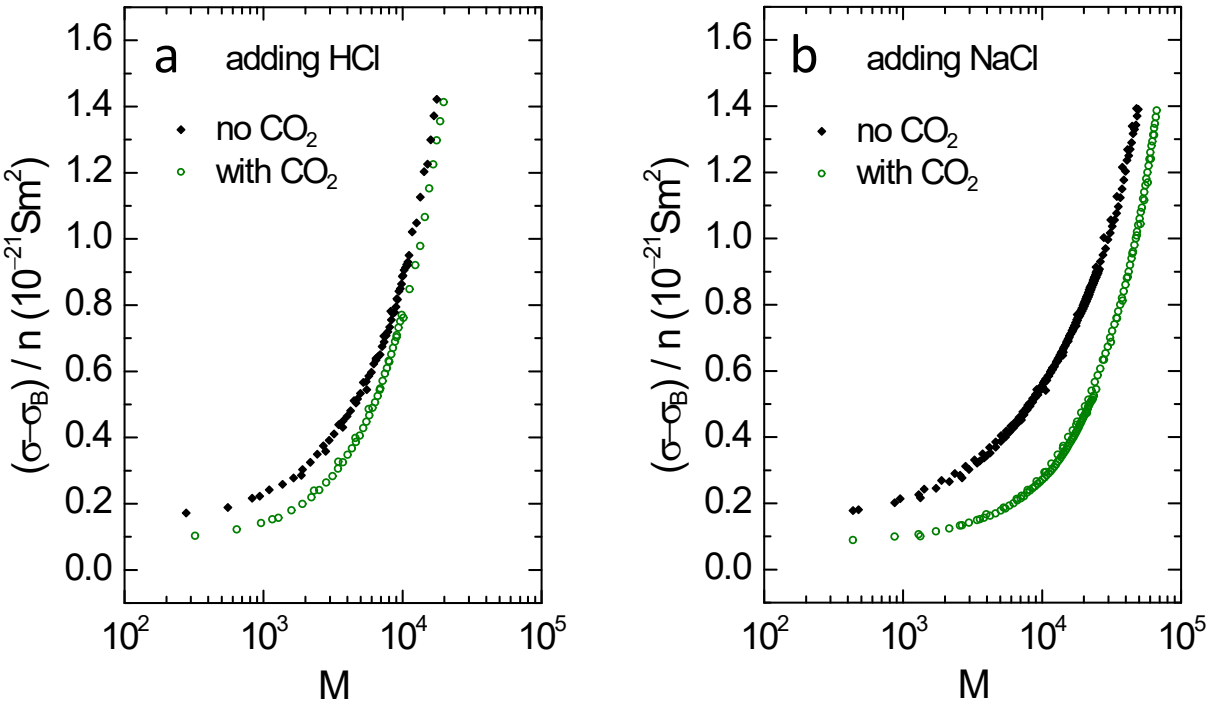

Figure S3 Background-corrected conductivity per particle in dependence on added electrolyte per particle. Starting conditions and type of added electrolyte are indicated in each key. For each experiment, the conductivities collapse on a single master curve over several orders of magnitude in *M*. Under ambient conditions (with CO_2), the conductivity contribution per particle is significantly lowered.

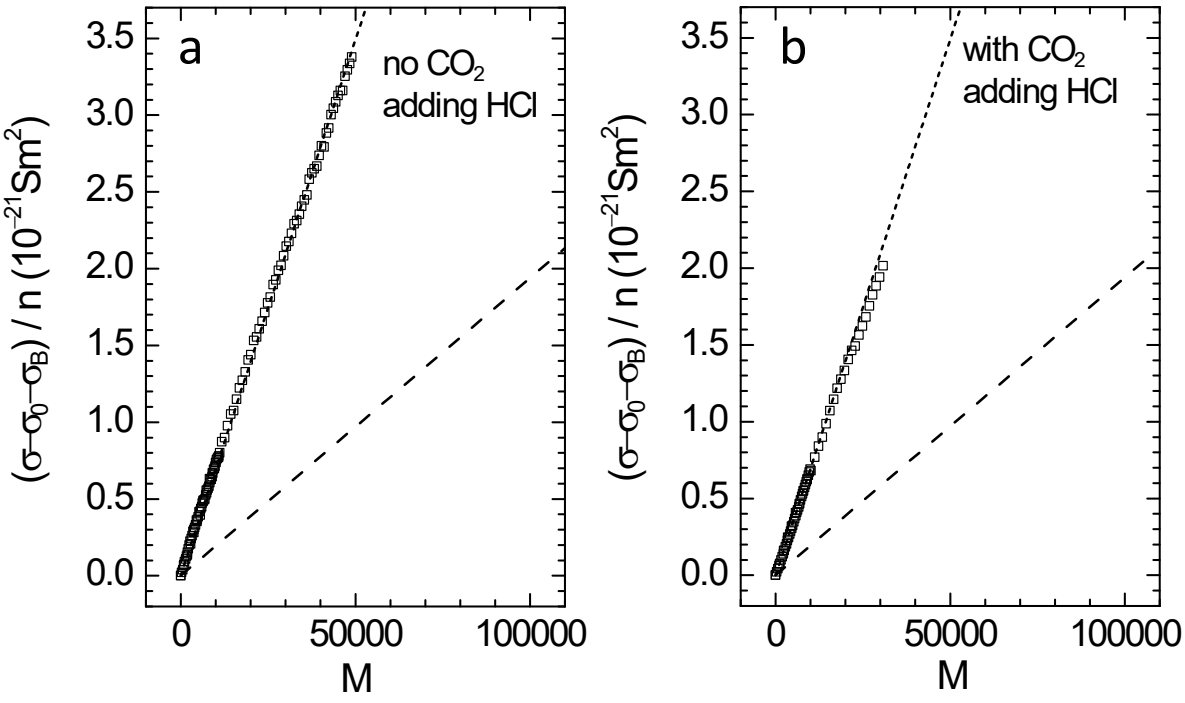

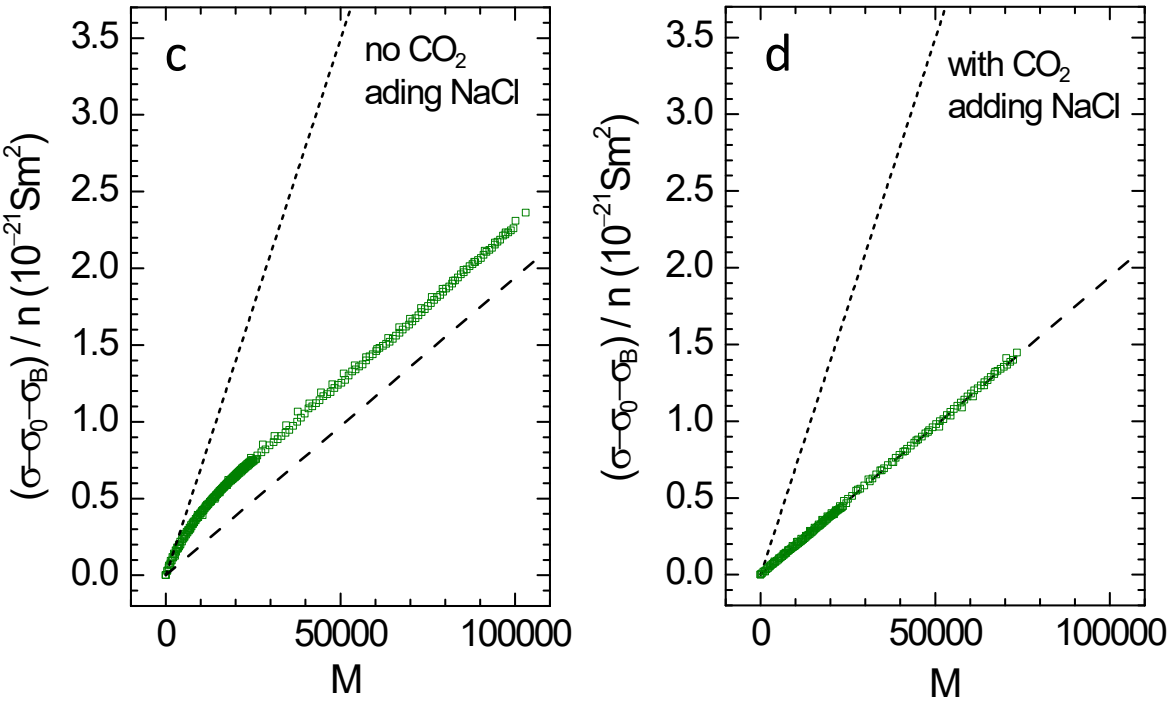

Figure S4. Conductivity contribution of added electrolytes per particle under different conditions. Data are plotted in dependence on the number of added electrolyte per particle. Starting conditions and type of added electrolyte are indicated in each key. For comparison, the dotted and dashed lines represent the limiting conductivity contribution of HCl and NaCl, respectively. (a) Addition of HCl in the absence of CO_2. (b) Addition of HCl in the presence of CO_2. (c) Addition of NaCl in the absence of CO_2. (d) Addition of NaCl in the presence of CO_2.

In Fig. S5, we replot the data of Fig. 4 in a double logarithmic fashion. The data for the addition of NaCl to a deionized and decarbonized suspension switch between the two limiting linear behaviors. The initial exchange of H^+ from the diffuse part of the EDL for Na^+ from the stagnant layer is nearly quantitative. It slows in the transition region, and for large M, it has practically ceased. In all other cases, a global fit of a power law with exponent 1 describes the data well. (The small deviation from linearity seen before in Fig. S4b is not discernible in this rendering).

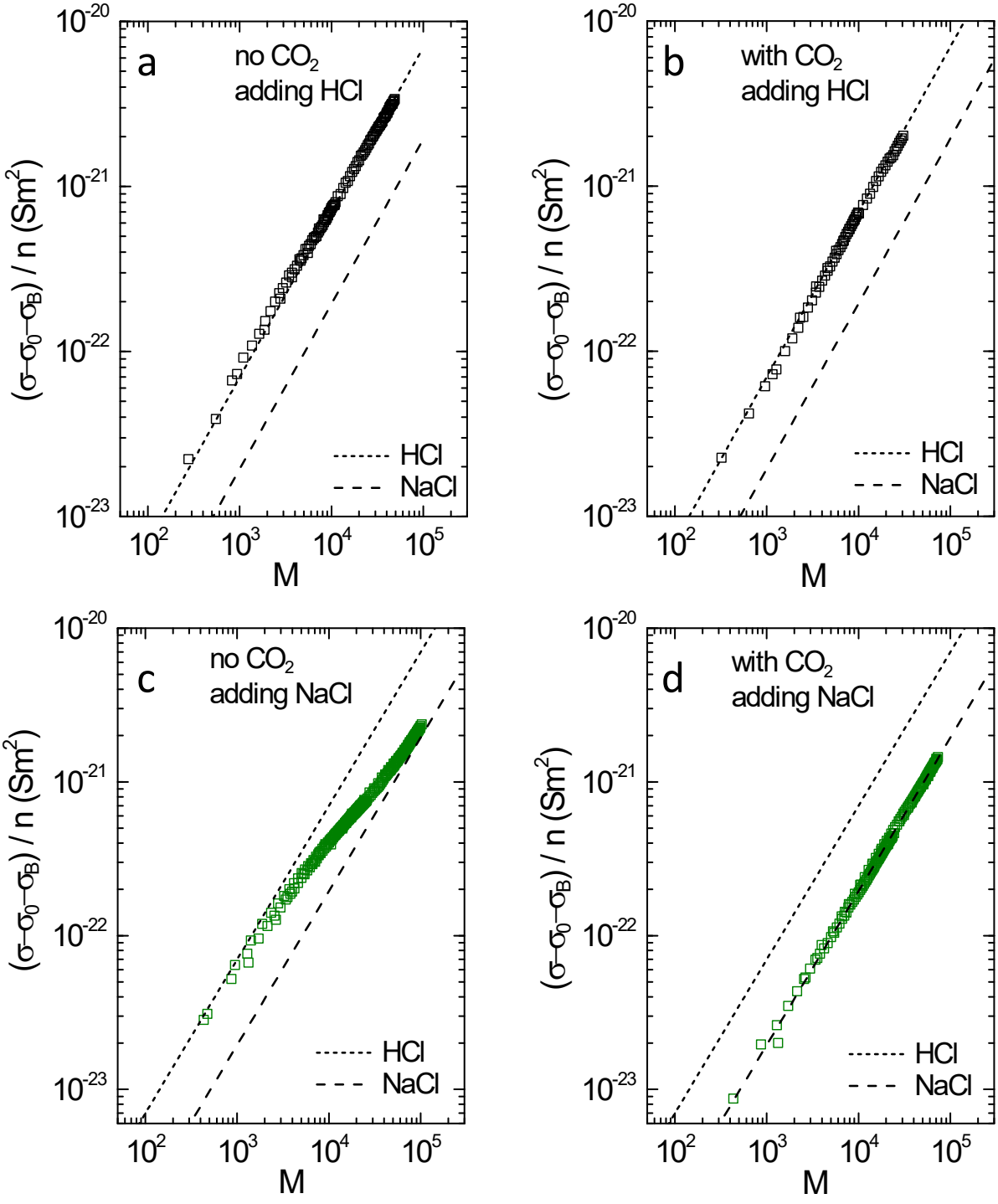

Figure S5. Conductivity contribution per particle in dependence on the number of 1:1 electrolyte ions added per particle. Data are plotted in a double logarithmic fashion. Starting conditions and type of added electrolyte are indicated in each key. The dotted and dashed lines represent the conductivity contribution of pure HCl and NaCl, respectively. (a) Addition of a HCl in the absence of CO_2. (b) Addition of HCl in the presence of CO_2. (c) Addition of NaCl in the absence of CO_2. (d) Addition of NaCl in the presence of CO_2.

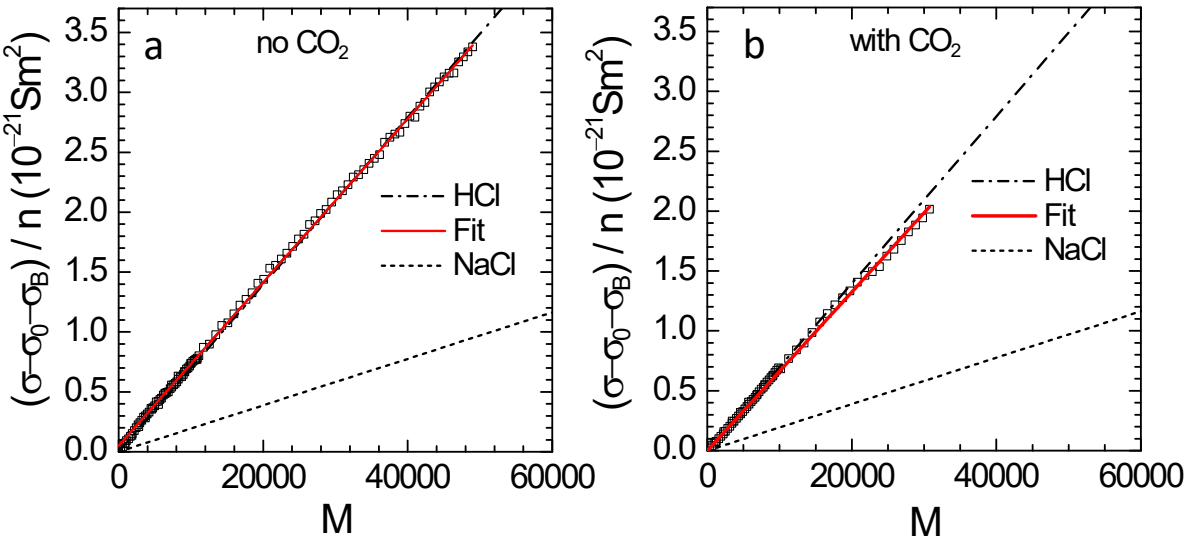

Figure S6. Conductivity contribution of an added simple acid under ideal (no CO_2) and environmental conditions (with CO_2). Also shown are least squares fits linear functions (red lines) do the data. As before, the dotted and dashed lines represent the conductivity contribution of pure HCl and NaCl, respectively. (a) Decarbonized conditions. Data are excellently described by the fit of Eqn (6) coinciding with the expectation for the conductivity contribution of HCl. (b) CO_2-saturated conditions. Within experimental scatter, data can again be described by a linear function, which, however does not coincide with the expectation for the conductivity contribution of HCl.

In the main text, we had compared the conductivity contribution of added NaCl to fits of Eqn (6). In Fig. S6, we show the corresponding data for the addition of HCl. Both data sets are excellently described by linear functions, signifying the absence of ion exchange. In fact, no exchange is anticipated for the addition of HCl, as the anion Cl^- anyway stays in the mobile part of the EDL, while the added cation H^+ is identical to the ion species of the stagnant part. Thus, $<\mu^+> = \mu_{H+}$, and there is no change in the average micro-ion mobility. Therefore, the slope in Fig. S6a coincides with that of the limiting conductivity contribution of HCl. In Fig. S6b, the slope falls slightly below this expectation. This can be attributed to additional pH driven charge regulation leading to a slight further reduction of Z and thus of Z_σ. A decrease of by pH driven charge regulation should also be present for the addition of HCl to a decarbonized system (Fig. S4a) but cannot not show up here, as Z_σ is already in the saturation regime.

The experiments were repeated using KCl and CsCl as added electrolytes to check for any influences of cation type on the exchange process. The corresponding data are shown together with Fits of Eqn (6) in Fig. S7. Using the conductivity charge of Z_σ = 2350 as input we obtain bare charges of $Z = (10.52 \pm 0.10) \times 10^3$ for KCl and $Z = (10.49 \pm 0.14) \times 10^3$ for CsCl. The double logarithmic data renderings show a transition between the two linear regimes with the turning point occurring around $M \approx 1 \times 10^4$.

Therefore, the data show exactly the same behaviour as seen for the addition of NaCl, and any influence of the type of cation can be excluded.

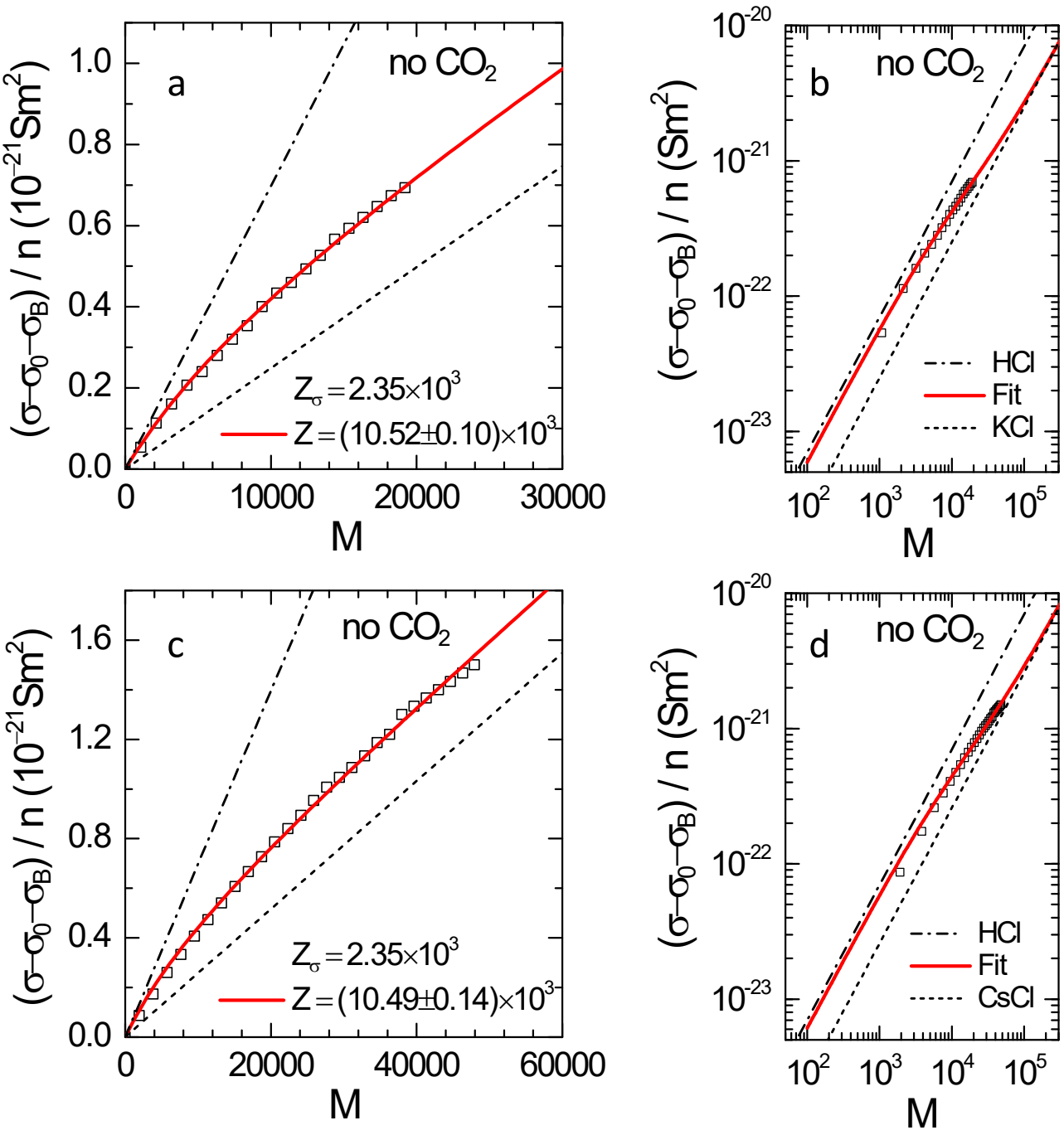

Figure S7. Conductivity contribution of added electrolytes under CO_2-free conditions for different cation types. The upper row shows data for the addition of KCl, the lower row shows data for the addition of CsCl. The data are plotted in dependence on the number of micro-ions added per particle. The red solid lines are least squares fits of Eqn (6) to obtain the corresponding particle bare charge, Z, as indicated in the keys. The dash-dotted and short dashed lines represent the limiting conductivity contribution of HCl, and of KCl and CsCl, respectively. (a) and (c) show linear, (b) and (d) show double logarithmic renderings of the data.

2. Dependence of Eqn. (6) on the charge ratio

The behaviour of Eqn. (6) is illustrated in Fig. S8 for selected charge ratios Z_σ/Z and $\sigma_B = 0$. Note that σ depends on Z entering via $\langle \mu^+ \rangle$. The first part of the electrolyte contribution goes to zero whenever $\langle \mu^+ \rangle$ equals μ_{H^+}. Our calculations show this to be the case in the limit of $M << Z$ and in particular at small charge ratio Z_σ/Z. Thus, the initial slope in a plot of $(\sigma-\sigma_0)/n$ versus M will correspond to the limiting conductivity contribution of HCl (dash-dotted line). Upon further addition of neutral electrolyte, the number of added Na^+ exchanged for H^+ decreases successively, while the number of counter-ions, Z, is conserved. In the limit of $M >> Z$, practically all immobilized H^+ have been exchanged for Na^+, ion exchange has ceased, and the slope approaches that of the limiting conductivity contribution of NaCl (short dashed line). The experimentally determined charge ratio was 0.23 corresponding roughly to the blue curve.

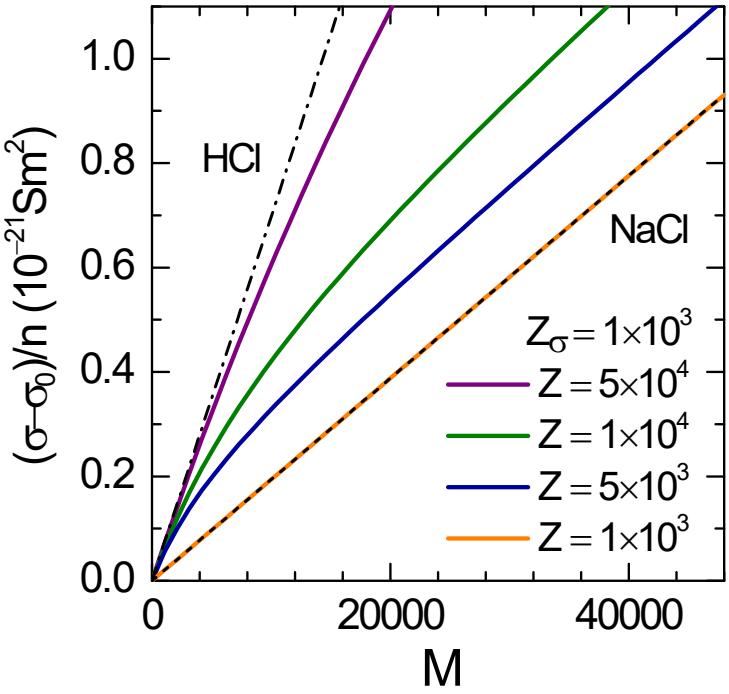

Figure S8. Conductivity contribution of added electrolytes. Model calculations using Equation (6) show the conductivity contribution per particle as function of the number small ions added per particle, M. The results for fixed effective charge and different bare charges are shown as color-coded solid lines, as indicated in the key. From top to bottom, the corresponding charge ratios are Z_σ/Z = 0.02, 0.1, 0.2, 1. We also show the two limiting linear regimes reached in systems with vanishing exchange. The limiting conductivity contribution of HCl (dashed-dotted line) is met for the addition of HCl irrespective of Z as long as $Z >> Z_\sigma$, as well as for addition of NaCl for $Z = \infty$. The limiting conductivity contribution of NaCl (dashed line) is met for addition of NaCl for $Z = Z_\sigma$.